Journal Pre-proof

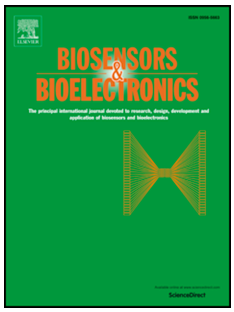

Detection of a secreted protein biomarker for citrus Huanglongbing using a single-walled carbon nanotubes-based chemiresistive biosensor

Thien-Toan Tran, Kelley Clark, Wenbo Ma, Ashok Mulchandani

PII: S0956-5663(19)30845-0

DOI: https://doi.org/10.1016/j.bios.2019.111766

Reference: BIOS 111766

To appear in: *Biosensors and Bioelectronics*

Received Date: 29 July 2019

Revised Date: 24 September 2019

Accepted Date: 7 October 2019

Please cite this article as: Tran, T.-T., Clark, K., Ma, W., Mulchandani, A., Detection of a secreted protein biomarker for citrus Huanglongbing using a single-walled carbon nanotubes-based chemiresistive biosensor, *Biosensors and Bioelectronics* (2019), doi: https://doi.org/10.1016/j.bios.2019.111766.

Detection of A Secreted Protein Biomarker for Citrus Huanglongbing Using A Single-Walled Carbon Nanotubes-Based Chemiresistive Biosensor

Authors: Thien-Toan Tran[1], Kelley Clark[2], Wenbo Ma[2], Ashok Mulchandani[1*]

****Corresponding Author***

Author affiliations:

[1]Department of Chemical and Environmental Engineering and Department of Materials Science and Engineering, UC Riverside

[2]Department of Microbiology and Plant Pathology, UC Riverside

1. Abstract

Citrus greening, or Huanglongbing (HLB), is currently the most devasting disease of citrus, creating unprecedented crisis for the multibillion-dollar global citrus industry. To-date, there is no effective cure and disease management relies on early detection and removal of infected trees. Thus, it is imperative that accurate, timely, and robust disease detection and diagnosis technologies are available to minimize the spread of disease. This study reports a sensitive and selective label-free biosensor that combines the physical and chemical advantages of carbon nanomaterials like single-walled carbon nanotubes (SWNTs) field-effect transistor (FET) / chemiresistor with selective antibodies against Sec-delivered effector 1 (SDE1), a secreted protein biomarker, for the detection of HLB. The biosensor detected SDE1 biomarkers for citrus greening in plant tissue extracts with the dynamic range over three orders of magnitude in the low nanomolar to micromolar concentration range and limit of detection of 5 nM. The study also demonstrated the use of the standard additions assay method with the biosensor to

attain a 90-percent signal recovery in concentrated plant tissue extract, allowing for quantitative detection without an external calibration. Adopting the novel detection strategy targeting the secreted protein biomarker, SDE1, addresses some of the challenges faced by current methods of nucleic acid-based assays and symptom-based diagnosis, which have been found prone to false negatives and misdiagnoses, respectively.

Key Words: Citrus huanglongbing; *Candidatus* Liberibacter asiaticus; Chemiresistor; Single-walled carbon nanotubes; Secretory biomarker; Standard addition method.

1. Introduction

Citrus greening disease, also known as Huanglongbing (HLB), is posing a worldwide threat to the multibillion-dollar citrus industry (Gottwald, 2010). Infected trees show dramatic fruit losses and will eventually decline. Other typical disease symptoms include yellow shoots, mottled leaves, and small, lopsided fruits that are green in color, hence the name "citrus greening". These fruits can often be off-tasting (Graça et al., 2016). HLB is associated with the bacterial species *Candidatus* Liberibacter, which colonizes the phloem tissues (i.e. vasculature) of infected plants (Bové, 2006; Gottwald, 2010; Teixeira et al., 2008). *Candidatus* Liberibacter spp. have yet to be obtained in pure culture, thus Koch's postulates have not been fulfilled and their association with HLB disease is based on metagenomic sequencing data and 16S rRNA analysis (Tyler et al., 2009). There are three species of *Candidatus* Liberibacter found to be associated with the disease: *Candidatus* Liberibacter asiaticus (*C*Las), *Candidatus* Liberibacter africanus (*C*Laf), and *Candidatus* Liberibacter americanus (*C*Lam). The various species are not constrained to the geographical regions based on their respective names with *C*Las being the most globally rampant in Asia and the Americas. The primary mode of transmission of the HLB

associated-pathogenic agents is through insect vectors, predominantly by the Asian and African citrus psyllids, *Diaphorina citri* and *Trioza erytreae*, respectively (Gottwald, 2010; Teixeira et al., 2008).

To-date, there are no cures for trees already infected with *C*Las. Management of the disease is focused on controlling its spread by eradication of infected trees and vectors (Bové, 2006; Gottwald, 2010; Pagliaccia et al., 2017). Thus, timely and accurate detection of infected plants is crucial. However, currently employed detection methods based on disease symptoms and nucleic-acid assays remain unsuccessful. Symptoms-based qualitative diagnosis of infected plants lacks accuracy due to variable latency of symptoms and similarity of symptoms to other citrus diseases and nutrient deficiencies (Bové, 2006). Assays for detection of nucleic acid biomarkers of *Ca*. Liberibacter could generate false negative results because they require the presence of the bacterial cells which are often unevenly distributed and exhibit low titers in infected plants (Teixeira et al., 2008; Irey et al., 2006; Ding et al., 2015). Furthermore, nucleic acid-based assays require laborious sample preparation and are costly and time-consuming, making these tools prohibitive for wide applications for disease management, especially when multiple samples need to be tested from one tree (Arredondo Valdés et al., 2016; Sankaran et al., 2010). Therefore, the detection of secreted, protein-based biomarkers of *C*Las provides a promising alternative to the current detection targets. A secreted protein of *C*Las, termed Sec-delivered effector 1 (SDE1), was discovered and studied by our group as a biomarker for HLB. SDE1 is unique to *C*Las and conserved across *C*Las isolates (Pagliaccia et al., 2017). This gene is highly expressed in infected citrus tissue at a relatively early infection stage, supporting early detection of HLB (Pagliaccia et al., 2017). Compared to the *C*Las bacterium, secreted SDE1 proteins are potentially systematically distributed throughout the infected trees via the phloem

flow. This wider distribution of SDE1 consequently would reduce the number of samples required to be collected from each tree. Thus, by adopting an affinity-based detection strategy using SDE1 as a biomarker, facile and reliable diagnosis of infected plants can be achieved.

In field-effect transistor (FET)/chemiresistor-based biosensors utilizing semiconducting single-walled carbon nanotubes (SWNTs), the single-layer surface atoms of the carbon nanomaterials are directly exposed to the environment, such that small alterations at the interface result in large changes in electrical properties of the nanomaterials (Liu and Guo, 2012). Furthermore, the nanoscale dimensions of these carbon nanostructures are comparable to the Debye length, the distance away from the sensor surface where the net electrostatic effects of charged molecules persist, ensuring successful electrical transduction of physical and chemical interactions at the SWNT surface. Biosensors employing an FET architecture and operation differ from conventional three-electrode electrochemical biosensor setup and operation, which typically has a working electrode, a reference electrode and a counter electrode (Balasubramanian and Burghard, 2006; Thévenot et al., 2001). The three-electrode setup of electrochemical biosensors are commonly utilized for measurement modes such as amperometry and potentiometry. The aforementioned electrochemical methods require electroactive species or biocatalytic elements to generate electrical responses (Lee et al., 2009; Thévenot et al., 2001). However, FET-based biosensors yield electrical responses upon affinity-based binding or adsorption of charged biomolecules with the semiconducting (transducer) channel without requiring electroactive analytes or biocatalytic elements, which highlights the potential of this biosensor architecture for label-free and affinity-based sensing. The electric field generated by charged biomolecules near the interface of the semiconducting material provides electrostatic gating effects on the channel that resemble the effects from applying a voltage potential to the

gate terminal of a transistor (Chen et al., 2019; Hao et al., 2019). Other electrical phenomena can result from such interfacial molecular interactions, such as modulation of the Schottky barrier (where metal-semiconductor junctions are present) and charge scattering (Heller et al., 2008). Similarly, a variation of the FET-biosensor architecture, is that of a chemiresistive biosensor which omits the gate electrode, allowing the modulation of the semiconducting channel conductance by the same mechanisms as in traditional FET-based biosensors with the external gating solely by the charged molecules near the interface of the semiconducting channel (He et al., 2012; Kaisti, 2017; Katz, 2004). Changes in electrical properties of the device, such as conductance or resistance, indicate physical and chemical alterations—due to analyte binding—of the surface properties of the carbon nanomaterials (Tlili et al., 2011).

In order for biosensors to have specificity to target analytes, biorecognition elements such as binding peptides, antibodies, aptamers, enzymes, complementary DNA oligomers, and molecularly imprinted polymers are required (Basu et al., 2015; Chen et al., 2019, 2017; Das et al., 2019; Gao et al., 2016; Kaisti, 2017; Okon and Ronkainen, 2017; Saylan et al., 2017; Terse-Thakoor et al., 2019). For SWNT-based FET and chemiresistive immunosensors, biorecognition elements are functionalized onto the surface of the transduction element, such as SWNTs, to specifically capture analyte molecules onto the surface of the transduction element (Tran and Mulchandani, 2016). The specific and selective localization of target analyte molecules at the surface and especially within the Debye length of the SWNT surface is essential for effective electrical transduction of analyte-capture events. Thus, the binding affinity and selectivity of the biorecognition molecules are critical to the overall sensor performance. Antibodies have been widely integrated in commercial immunoassays and affinity-based biosensor platforms for detection of biomarkers in complex samples (Conroy et al., 2009; Jain et al., 2019). Custom

novel antibody generation can be achieved within reasonable costs and time, where large-scale production methods are available, making antibody-based detection a rational and viable strategy in biosensor development (Conroy et al., 2009; Sharma et al., 2016).

Thus, this study reports a sensitive antibody-based chemiresistive biosensor for detection of SDE1 biomarkers for citrus greening. Applying the advantages of nanoscale chemiresistor-based biosensors using semiconducting SWNTs and incorporating the biomarker strategy using the *C*Las-specific SDE1 protein allowed the development of a novel label-free chemiresistive biosensor platform for the detection of *C*Las. To impart specificity to the biosensor, SWNTs were functionalized with custom-generated anti-SDE1 polyclonal antibodies (Pagliaccia et al., 2017). The biosensor showed high sensitivity and specificity for the SDE1 biomarker in phosphate buffer and citrus plant tissue extracts with dose-dependent response.

2. Materials and Methods

3.1 Reagents and Materials

All materials and chemicals were purchased from Fisher Scientific unless specified otherwise. Recombinant HLB biomarker, SDE1, and anti-SDE1 polyclonal antibodies (pAb) were prepared according to previously reported method (Pagliaccia et al., 2017). 95% 3-Aminopropyl-triethoxysilane (APTES), 1-Pyrenebutyric acid N-hydroxysuccinimide ester (95%) (PBASE), anhydrous N,N-dimethylformamide (DMF), and ethanolamine were obtained from Sigma-Aldrich (St. Louis, Mo, USA). Tween-20 was obtained from Bio-Rad (Irvine, CA, USA). Highly p-doped 4-inch silicon wafers with 300 nm thermal oxide layer were purchased from Ultrasil Corporation (Hayward, CA, USA). 95% semiconducting SWNTs solution supplied at 10 μg/mL was purchased from NanoIntegris, Inc. (Quebec, Canada). SWNTs solution was

138 further diluted in the same surfactant solution (proprietary information) to 2.5 µg/mL for device
139 fabrication. 10 mM phosphate buffer (PB) pH 7.4 was prepared from monobasic and dibasic
140 sodium phosphate salts and pH-adjusted with dilute hydrochloric acid and sodium hydroxide.

141 **3.2 Device Fabrication**

142 As presented in the scheme in Figure S1, photolithography and lift-off processes were
143 used for patterning of 10-µm gap gold (Au) microelectrodes onto Si/SiO_2 wafer in the cleanroom
144 at the Center for Nanoscale Science and Engineering, University of California, Riverside (UCR).
145 Briefly, microelectrodes with 10 µm by 10 µm gap size were defined onto Si/SiO_2 wafer using
146 photolithography with Shipley 1813 positive photoresist. E-beam evaporation was employed to
147 deposit 10 nm thick chromium (Cr) adhesion layer and 100 nm thick Au followed by acetone
148 wash to remove excess photoresist and Cr-Au layers, leaving multiple patterns of the
149 microelectrodes. After cutting individual chips from the wafers, the chips were cleaned with
150 acetone and isopropyl alcohol (IPA) and then dried under a stream of nitrogen.

Next, to prepare SWNT transduction channels across the patterned source and drain electrodes, the SiO_2 surface was first functionalized with a self-assembled monolayer of (3-aminopropyl) triethoxysilane (APTES) which aids in the assembly of SWNT network on the surface of our sensor as shown in Figure 1. After APTES functionalization, a 10 µm by 50 µm rectangular region of APTES overlapping two electrodes was photolithographically patterned by first using Shipley 1813 photoresist to protect the rectangular region, followed by reactive ion etching on an Oxford Plasmalab 100/180 etcher of unprotected surfaces to remove excess APTES outside of the 10 µm by 50 µm regions. Subsequently, the protective Shipley 1813 photoresist was removed to re-expose 10 µm by 50 µm rectangular region of APTES using an acetone bath, followed by washing with IPA, and drying with nitrogen.

Five µL SWNT solution was drop-casted onto the patterned APTES region and the droplet was allowed to dry in air overnight. The anionic surfactant molecules, which are physisorbed to the SWNTs, are electrostatically attracted to the amino groups of the APTES covered surface, which consequently anchors the SWNTs onto the APTES-functionalized SiO_2 surface (Choi et al., 2000; Liu et al., 1999; Sarkar and Daniels-Race, 2013). Washing the device with distilled water removes excess unbound and weakly bound SWNTs and excess surfactant molecules from the sensor surface. The assembled SWNTs were then annealed in air at 250^{o}C to burn off detergent molecules coating SWNTs leaving surfaces free for further bioreceptor/antibody functionalization. Next, the gold source and drain electrodes were passivated by incubating the device with 100 mM 6-mercapto-1-hexanol diluted in anhydrous ethanol (200 proof) for 1 hour at room temperature, followed by rinsing in ethanol and blow-drying under a stream of nitrogen. The functionalization of SWNT surfaces with antibodies was started with modification with PBASE linker molecules by incubation with 3.0 mg/mL of

PBASE reagent in DMF for 1 hour at room temperature followed by drop-casting 20 µL of 50 µg/mL of anti-SDE1 antibody in PB onto the SWNT sensing region and incubated overnight at 4°C. The biosensor was then blocked with bovine serum albumin at 10 mg/mL in PB for 1 hour, followed by reaction with 100 mM ethanolamine in pH 8.0, 10 mM phosphate buffer to quench unreacted succinimidyl esters and then bare and unfunctionalized SWNT regions were blocked with 1% (w/v) of Tween-20 surfactants for 1 hour. These quenching and blocking steps minimize non-specific binding of biomolecules to the sensor.

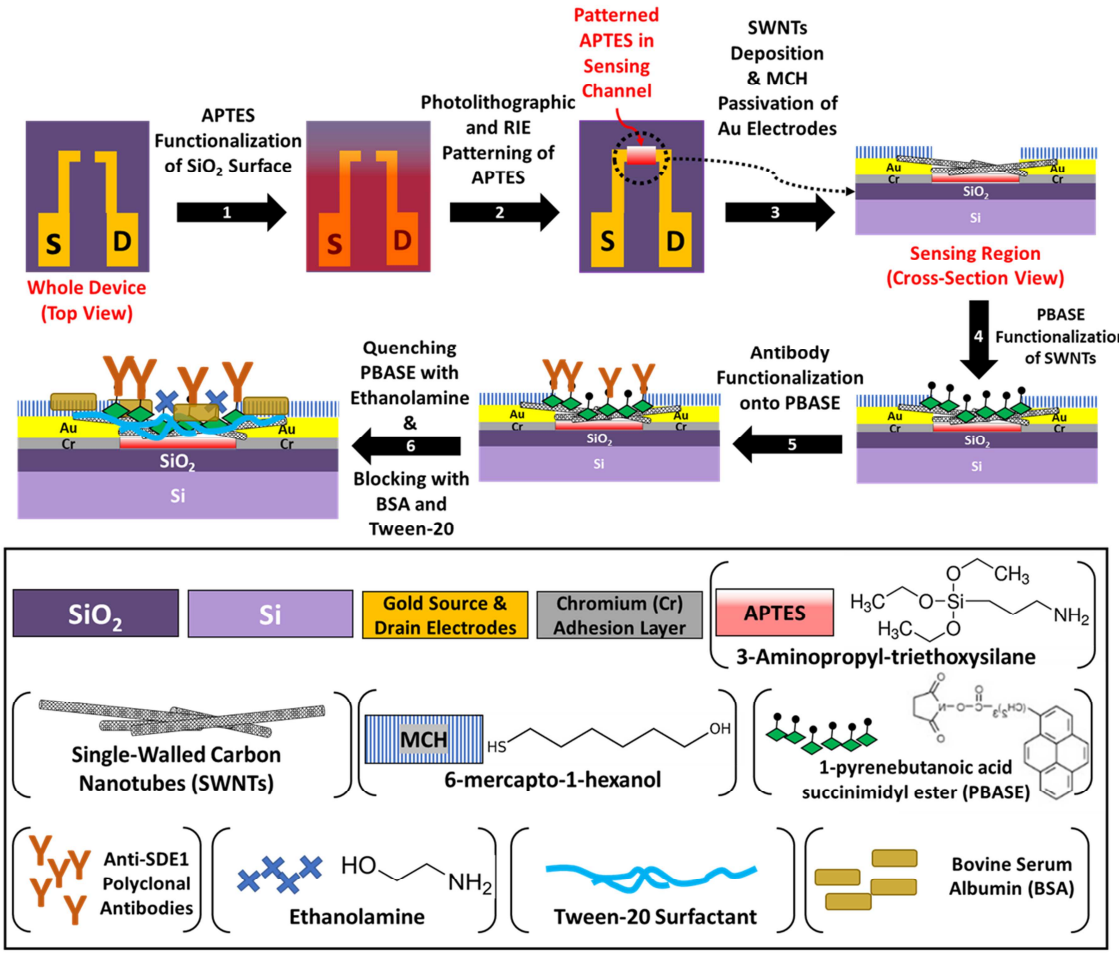

***Figure 1**: Schematic diagram illustrating fabrication and functionalization process for SWNT-based chemiresistor devices. Figures are not drawn to scale.*

3.3 Electrical Measurement and Biosensing Protocols

Electrical measurements were performed using a Keithley 2636B source and measurement unit. Measurements were multiplexed across multiple devices using an in-house built multiplexer system based on the Arduino Mega 2560 microcontroller and relay boards. LabVIEW software was used to control measurement instruments and for data acquisition. Current versus time (I-t) measurements were performed at a fixed source-drain potential (V_{SD}) of +0.1 V. I-t measurements were achieved by sequentially measuring each biosensor at 0.5-second intervals using the multiplexer unit. Resistance versus time (R-t) curves values were then obtained by dividing the 0.1 V (applied V_{SD}) by each measured I_{SD} value at each time. Current versus voltage (I-V) measurements were obtained by applying a sweeping source-drain potential (V_{SD}) from -0.1 V to +0.1 V with 0.01 V step size, while measuring source-drain current (I_{SD}). Back-gated FET measurements were conducted by using the p-doped silicon as the bottom gate electrode and sweeping the gate potentials (V_{BG}) with a constant V_{SD} bias of 0.1 V and measuring I_{SD} and gate-drain leakage current ($I_{leakage}$).

R-t measurements were used to monitor real-time current responses of each SWNT biosensor to various samples and concentrations of SDE1 protein. Prior to biosensing experiments, a silicone well with pressure sensitive adhesive was placed over the biosensor to prevent overflowing of samples outside the sensing region. Biosensing experiments and measurements were conducted at room temperature in a humid chamber. For SDE1 detection in PB, 15 μL of PB was initially drop-casted gently onto the sensing area. After allowing SWNT biosensor current response to stabilize within 10 to 15 minutes, sequential additions of 1 to 2 μL of samples were pipetted into the 15 μL PB drop with gentle mixing by aspiration with the same micropipette. SDE1 samples in PB with increasing concentrations were sequentially added this way in 15- to 30-minute intervals to allow for stable current responses. For SDE1 detection in

plant tissue extract, SDE1 proteins were spiked into 10% plant tissue extract to simulate real samples. Firstly, 15 μL of PB was drop-casted gently onto the sensing area. The sensor was then pre-conditioned to the sample matrix by adding another 15-uL drop of the plant tissue extract (without SDE1 protein) into the droplet with gentle mixing by pipette aspirations. After allowing SWNT biosensor current response to stabilize within 30 minutes, additions of 1 to 2 μL of SDE1 in plant tissue extract were pipetted onto the sensing area with gentle mixing by aspiration with the micropipette. Total SDE1 concentrations were calculated for each sample addition to account for changes in volume of the sample solution on the biosensor.

Calibration curves for multiple biosensors were obtained by averaging normalized resistance changes ($\Delta R/R_i$) at each sample condition. More specifically, resistance over time measurement for each biosensor was averaged over 30 measurements (approximately 60 seconds intervals) and the resistance changes were calculated using the equation

$$\frac{\Delta R}{R_i} = \frac{R_f - R_i}{R_i} \quad (1)$$

where R_f is the equilibrated resistance after each addition and R_i is the equilibrated resistance of the initial PB addition and the initial biosensor precondition step for detection of SDE1 in PB and in plant tissue extract, respectively.

3.4 Citrus Sample Preparation

Stem samples from healthy young branches were cut into small sections and grounded to fine powder as previously described (Pagliaccia et al., 2017). Grounded tissue was then suspended in PB at 1.0 g/mL and vortexed to mix. Supernatants (i.e. extract) were obtained by centrifuging the suspensions at 13,800 x *g* for 5 minutes. Supernatants were then syringe-filtered with 0.2-μm membrane pore size to remove large plant debris. For biosensing experiments, supernatants were then diluted in PB to 10% v/v.

4 Results and Discussion

4.1 Device Characterization

Carbon nanotubes can be considered a 1-dimensional allotrope of carbon, which can be described as a ribbon of graphene comprising sp^2 hybridized carbon atoms with a hexagonal lattice seamlessly rolled into a cylindrical tube (Iijima, 1991; Watson, 2007). Single-walled carbon nanotubes (SWNTs) have one single layer of sp^2 carbon atoms forming the nanotube (Iijima, 1991; Odom et al., 1998). SWNTs can have either semiconducting or metallic electronic properties depending on their chirality and diameter (Hu et al., 2010). Back-gated FET measurements of our SWNT devices confirms p-type semiconductor behavior of SWNTs where the major charge carriers are holes (Figure S2). This is evident as I_{SD} value increased with more negative gate voltages which p-dopes the semiconducting SWNT channel enhancing the number of hole charge carriers. Conversely, more positive gate voltages n-dopes the SWNT channel, leading to depletion of the major hole charge carriers as seen by lower I_{SD} values (Heller et al., 2008; Ohno et al., 2010; Tran and Mulchandani, 2016). Leakage current was shown to be negligible (average $I_{Leakage} = 24 \pm 70$ nA) compared to source-drain current ($I_{SD} > 10^4$ nA). Using scanning electron microscopy (SEM) on a Leo SUPRA-55 instrument at the Center for Nanoscale Science and Engineering at UCR, the preferential deposition of SWNTs onto APTES-patterned SiO_2 surface of the biosensor was confirmed. As shown in Figure 2, monodispersed SWNTs self-assembled onto the 10 μm by 50 μm rectangular APTES region with much higher density and uniformity than SiO_2 surfaces without APTES. Thus, by photolithographic patterning and RIE of the APTES self-assembled monolayer prior to dropcasting of SWNTs, preferential assembly of SWNTs at the microscale level in specific regions of the device is attainable after washing away unbound excess SWNTs. This fabrication process allows for

precise microscale control of SWNTs deposition at desired locations without additional exposure of the SWNTs to photolithographic processes that may lead to undesired chemical residues of SWNT surfaces.

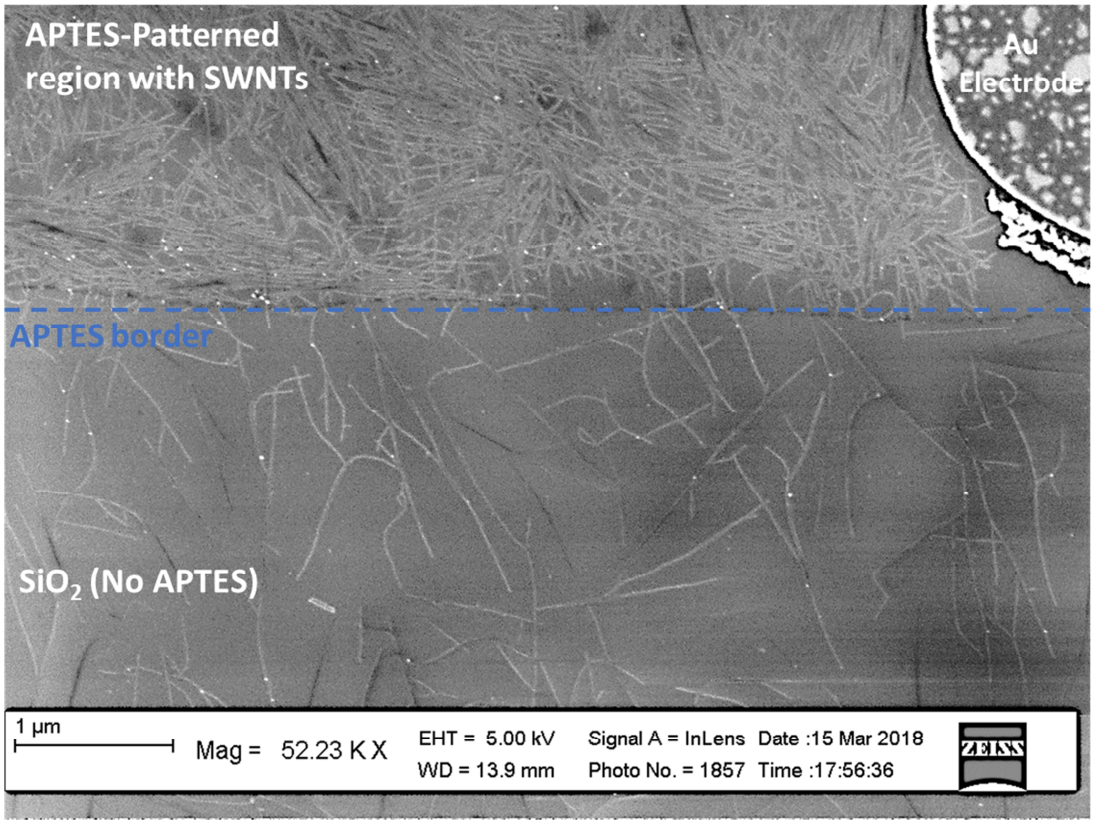

***Figure 2**: SEM image of SWNTs deposited onto APTES-patterned SiO_2 surface with preferential self-assembly on APTES-functionalized areas versus bare SiO_2 areas.*

To achieve specific detection of analyte molecules, the SWNTs require functionalization with the biorecognition elements (e.g. antibodies, enzymes, aptamers, and other binding peptides, etc.). Modification of SWNTs with the biorecognition molecules is achieved through various chemical means that can be categorized as direct covalent conjugation to the carbon nanostructure or through non-covalent conjugation to the nanostructure (Banerjee et al., 2005; Sun et al., 2002; Tran and Mulchandani, 2016). One major disadvantage of covalent functionalization of SWNTs is the alteration of electronic structure and properties of the

nanotubes due to disruption of carbon sp^2 bonds (Banerjee et al., 2005; Georgakilas et al., 2012). Therefore, non-covalent functionalization strategy was selected. Non-covalent conjugation of biomolecules onto sp^2 carbon bond-rich SWNT surfaces was performed by bi-functional linker molecule, 1-pyrenebutanoic acid succinimidyl ester (PBASE). The π-electron-rich pyrenyl group π-stacks with the carbon nanostructure while the succinimidyl ester group specifically reacts with amine groups on the biorecognition molecule to form an amide bond. After functionalizing the carbon nanomaterials with the desired biorecognition molecules, unreacted chemical moieties and carbon surfaces were chemically quenched and physically blocked to block/minimize non-specific binding during sensing procedure. The various functionalization steps were monitored using I-V measurements as shown by I-V characteristics of a representative device (Figure S3). Due to the sensitivity of the succinimidyl ester of PBASE linkers to hydrolysis, I-V measurement after PBASE functionalization was omitted to allow for immediate incubation with the anti-SDE1 antibodies for further bioreceptor immobilization. After antibody conjugation to the SWNT surface via PBASE linker, a large decrease in the slope of the I-V measurements (i.e. increase in device resistance) from bare SWNTs was observed. While PBASE linkers have been shown to contribute to changes in p-type SWNT device resistance by electron donation and charge scattering, subsequent biomolecule conjugation to PBASE consistently yield more significant changes in the slopes of I-V curves due to the much larger size of protein molecules indicating increased device resistance (García-Aljaro et al., 2010; Ramnani et al., 2013; Wasik et al., 2018). Subsequent quenching and blocking steps led to additional increase in the device resistance.

285 **4.2 Detection of SDE1 HLB Biomarker**

286 After SWNT biosensors were functionalized with anti-SDE1 antibodies and blocked, the
287 devices were then used for biosensing experiments. Figure S4 shows a representative real-time
288 response of a single biosensor for detection of SDE1 spiked in PB. The sensor response ($\Delta R/R_i$)
289 was normalized to the resistance of the initial addition of 15 μL PB. Electrical responses were
290 measured for each biosensor in response to the various additions of negative controls samples
291 and/or SDE1 proteins. Upon specific intermolecular interactions between SDE1 molecules with
292 functionalized anti-SDE1 antibodies at the surface of the SWNTs, one or more of the following
293 mechanisms are known to contribute to the modulation of electrical properties (i.e. measured
294 electrical responses) of SWNT-FET biosensors: (1) surface charge-induced gating effect or
295 electrostatic gating, (2) charge transfer between the biomolecules and the carbon nanomaterials,
296 (3) charge scattering across the carbon nanomaterials, and (4) Schottky barrier modification
297 occurring between the carbon nanomaterials and metal electrodes (Byon and Choi, 2006; Chen et
298 al., 2005; Heller et al., 2008; Liu and Guo, 2012; Ohno et al., 2015; Tran and Mulchandani,
299 2016). To elucidate which mechanism(s) contribute to observed sensor responses and the degree
300 to which the mechanism(s) influence our sensor responses requires extensive mechanistic study
301 and modeling. However, through systematic investigations of SWNT-based FET biosensors,
302 Heller et al. had suggested that the two major sensing mechanisms of these biosensors are from
303 electrostatic gating effect and modulation of the Schottky barriers (Heller et al., 2008).

304 From the R-t measurements, it was observed that three sequential additions of 1 μL PB
305 (blank controls) produced little to no change in sensor response after allowing for 10 minutes for
306 stabilization from the physical perturbation. Furthermore, as summarized in Figure 3, even after
307 additions of much higher concentrations of bovine serum albumin (BSA) negative controls at

790 nM and 1500 nM, average sensor responses for 5 devices ($\Delta R/R_i$ = 0.04 ± 0.02 and $\Delta R/R_i$ = 0.05 ± 0.02, respectively) were significantly lower compared to sensor responses to 34 nM of SDE1 ($\Delta R/R_i$ = 0.23 ± 0.08). This is indicative of the specificity of our biosensors for SDE1. A calibration curve was generated from the averaged normalized resistance responses

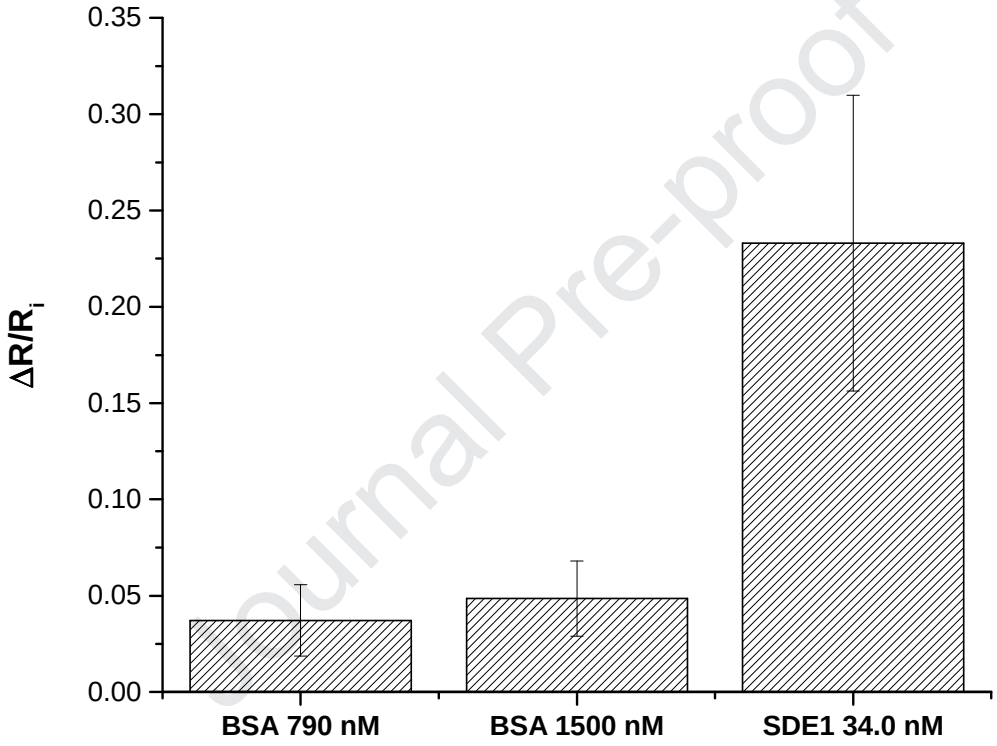

***Figure 3**: Normalized resistance responses of SWNT biosensors to high concentrations of nonspecific bovine serum albumin (BSA) proteins at 790 nM and 1500 nM compared to much lower concentration of SDE1 antigen. Devices were functionalized with anti-SDE1 antibodies. Each data point represents the average normalized resistance from multiple independent biosensors. Error bars represent ±1 standard deviation from 5 biosensors (n = 5).*

of these 5 sensors as shown in Figure 4. The data points were fitted to a 4-parameter logistic model using the following function

$$y = \frac{A1-A2}{\left[1+\left(\frac{x}{x_0}\right)^p\right]} + A2 \qquad (2)$$

as recommended for ligand-binding assays (Fakanya et al., 2014; Findlay and Dillard, 2007; O'Connell et al., 1993), where *y* represents the normalized change in resistance (i.e. sensor response), *x* is the independent variable (SDE1 concentration), *A1* is the maximum value of the calibration curve, A2 is minimum value of the calibration curve, x_0 is the concentration

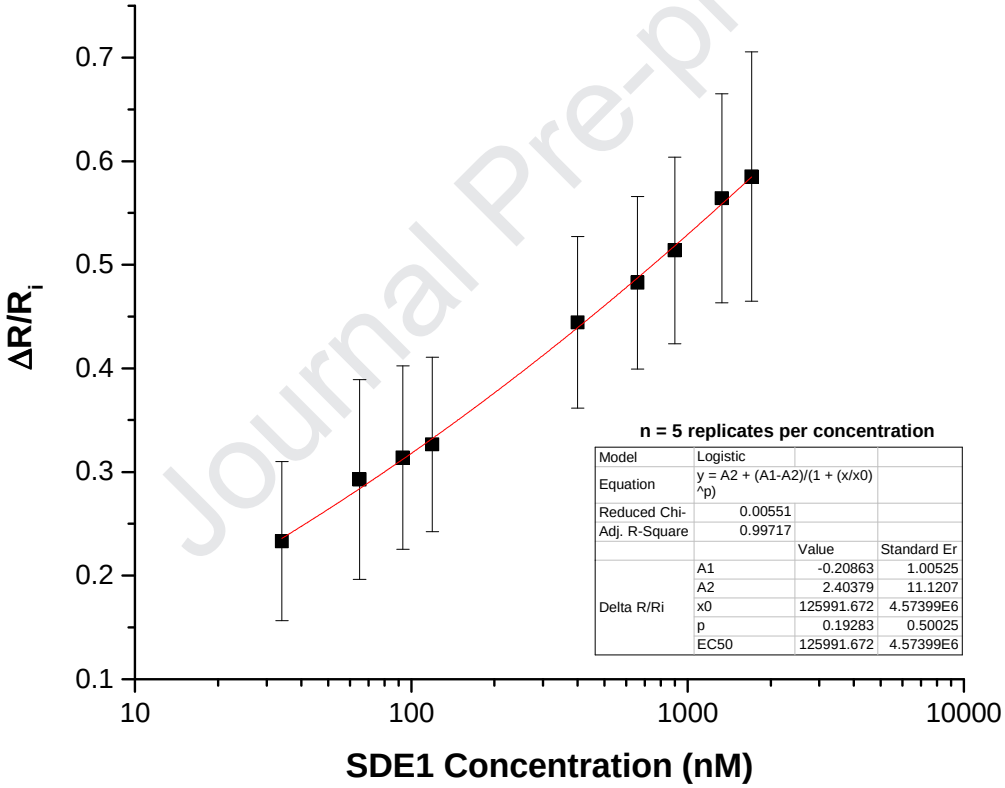

Figure 4*: Calibration plot of SDE1 proteins in 10 mM phosphate buffer, pH 7.4. Resistance changes were calculated using the equation* $\frac{\Delta R}{R_i} = \frac{R_f - R_i}{R_i}$ *where* R_f *is the equilibrated resistance after each addition, and* R_i *is the equilibrated resistance of the initial PB addition. Data was fitted using 4-parameter logistic regression analysis. Data points represent the averaged normalized measurements from 5 (n = 5) independent SWNT biosensors. Error bars represent ±1 standard deviation.*

at EC_{50}, and *p* is the slope at $x = x_0$. From the calibration curve in Figure 4, the biosensors

showed a dynamic response range of tens of nanomolar to micromolar concentrations of SDE1 biomarker. The limit of detection, based on the three times the signal-to-noise of the blank (0 nM SDE1), was estimated to be less than 1 nM of SDE1.

In order simulate detection of the SDE1 HLB protein biomarkers in real plant tissue samples, plant extracts prepared from healthy (uninfected and hence without SDE1 proteins) grapefruit leaves were used as the sample matrix. SDE1 proteins were spiked into the plant extract at various concentrations for biosensor experiment. The biosensors were conditioned by adding 15 μL of healthy plant tissue extract to the 15 μL of PB on the sensing area for 30 minutes until the sensor response stabilized. By allowing the sensor to equilibrate to the more complex plant extract matrix, background responses from the biomolecule-rich extract were avoided, reducing their interfering effects. Before proceeding to additions of SDE1-spiked plant extract samples, a stable baseline response was verified by adding another 10 μL of plant extract (without SDE1 proteins) and where no significant change was observed for the normalized sensor response ($\Delta R/R_i$ = -0.03 ± 0.05) from the baseline ($\Delta R/R_i$ = 0.00 ± 0.01) for 5 devices (n = 5). Next, sequential additions of samples with SDE1 spiked in plant extract were performed. Figure S5 shows the normalized real-time sensor response for a representative biosensor for detection of SDE1 biomarker in complex plant tissue extract. All biosensors showed similar increase in resistance responses to each addition of SDE1 in plant tissue extract, which is consistent with SDE1 detection in PB. Biosensing results in simple phosphate buffer and in plant tissue extract showed that with increasing concentration of SDE1 biomarkers, there is an increase in device resistance suggesting there are net positive charges presented on the surfaces of antibody-bound SDE1 proteins which induced electrostatic gating (via n-doping) of the p-type SWNT channel causing the decrease in device conductance (Heller et al., 2008). Furthermore,

due to the chemical blocking of the gold electrodes MCH to prevent non-specific binding at the junction between the electrode and SWNT channel, this minimizes the contribution of Schottky barrier effect in the overall electrical sensor responses (Chen et al., 2004; Heller et al., 2008; Wasik et al., 2018). The dose-dependent sensor responses to increasing concentrations of SDE1 biomarker in the presence of plant extract suggests the biosensors are indeed specific to SDE1 HLB biomarkers even in the complex plant tissue matrix. A calibration curve was generated from the averaged normalized resistance responses of these 5 sensors (Figure 5). The data points were fitted to a 4-parameter logistic model as recommended for ligand-binding assays with a dynamic response range of few nanomolar to few micromolar concentrations of SDE1 biomarker in plant extract which is similar to that of SDE1 detection in PB (Fakanya et al., 2014; Findlay and Dillard, 2007; O'Connell et al.,

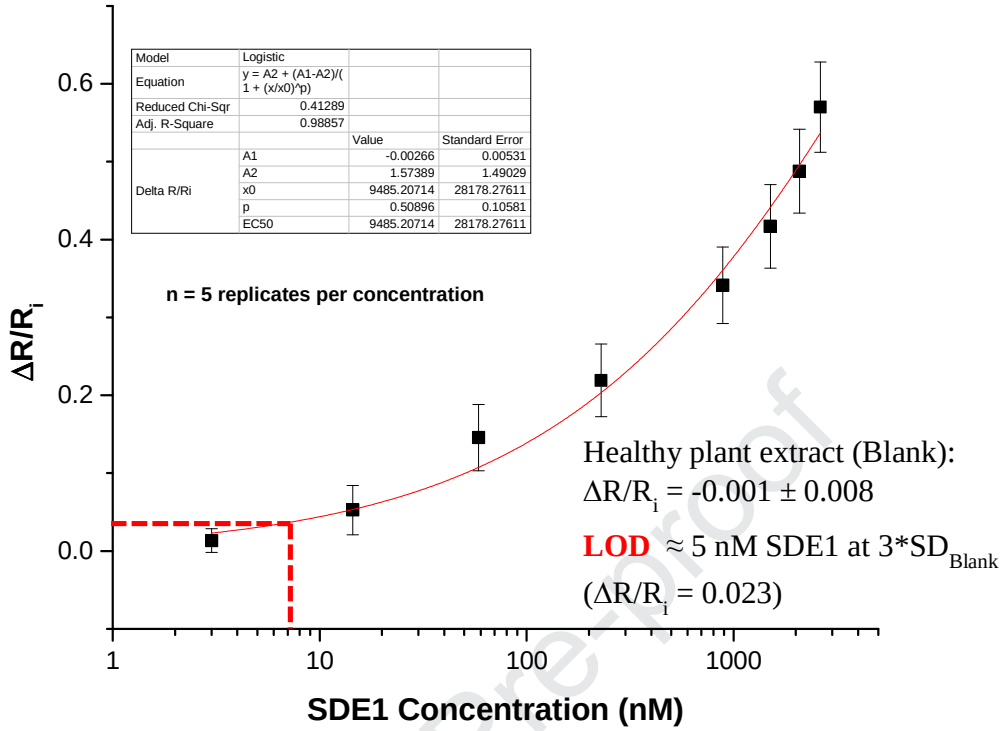

***Figure 5**: Calibration plot of SDE1 proteins in 10 mM phosphate buffer, pH 7.4. Resistance changes were calculated using the equation* $\frac{\Delta R}{R_i} = \frac{R_f - R_i}{R_i}$ *where* R_f *is the equilibrated resistance after each addition, and* R_i *is the equilibrated resistance after device conditioning with healthy plant tissue extract. Data was fitted using 4-parameter logistic regression analysis. Data points represent the averaged normalized measurements from 5 (n = 5) SWNT biosensors. Error bars represent ±1 standard deviation.*

1993). The limit of detection, based on 3 times the signal-to-noise (0 nM SDE1), was determined to be 5 nM of SDE1. While the trends for the calibration curves of SDE1 detection in PB and detection in plant extract are positive, the two calibration curves do not exactly align and have different values for the four parameters A1, A2, x_0, and p fitted using the 4-parameter logistic function. This may be due to some persistent matrix effect of the plant tissue extract.

One strategy to resolve for matrix effects is to use the standard addition method (Andersen, 2017; Ellison and Thompson, 2008). To resolve matric effect of plant tissue extract, four solutions containing 0, 10, 20 and 30 nM of SDE1 proteins in healthy plant tissue extracts

mixed with a simulated “unknown” plant extract sample spiked with 29.4 nM SDE1 were prepared. Applying these samples onto the immunosensors and measuring the normalized $\Delta R/R_i$ allowed generation of a standard addition curve to calculate the original concentration of the “unknown” plant extract sample of 26.4 nM (Figure 6). The measured concentration using the standard addition is within 90 percent of the theoretical concentration of the simulated unknown sample. This suggests that the method of standard additions is a viable assay method for mitigating plant extract matrix effects without requiring an external calibration curve.

Solution Number	Concentration of Standard Addition (nM)	ΔR/Ri	Standard Deviation (n = 5)
1	0	0.032	0.006
2	10	0.050	0.009
3	20	0.062	0.010
4	40	0.085	0.021

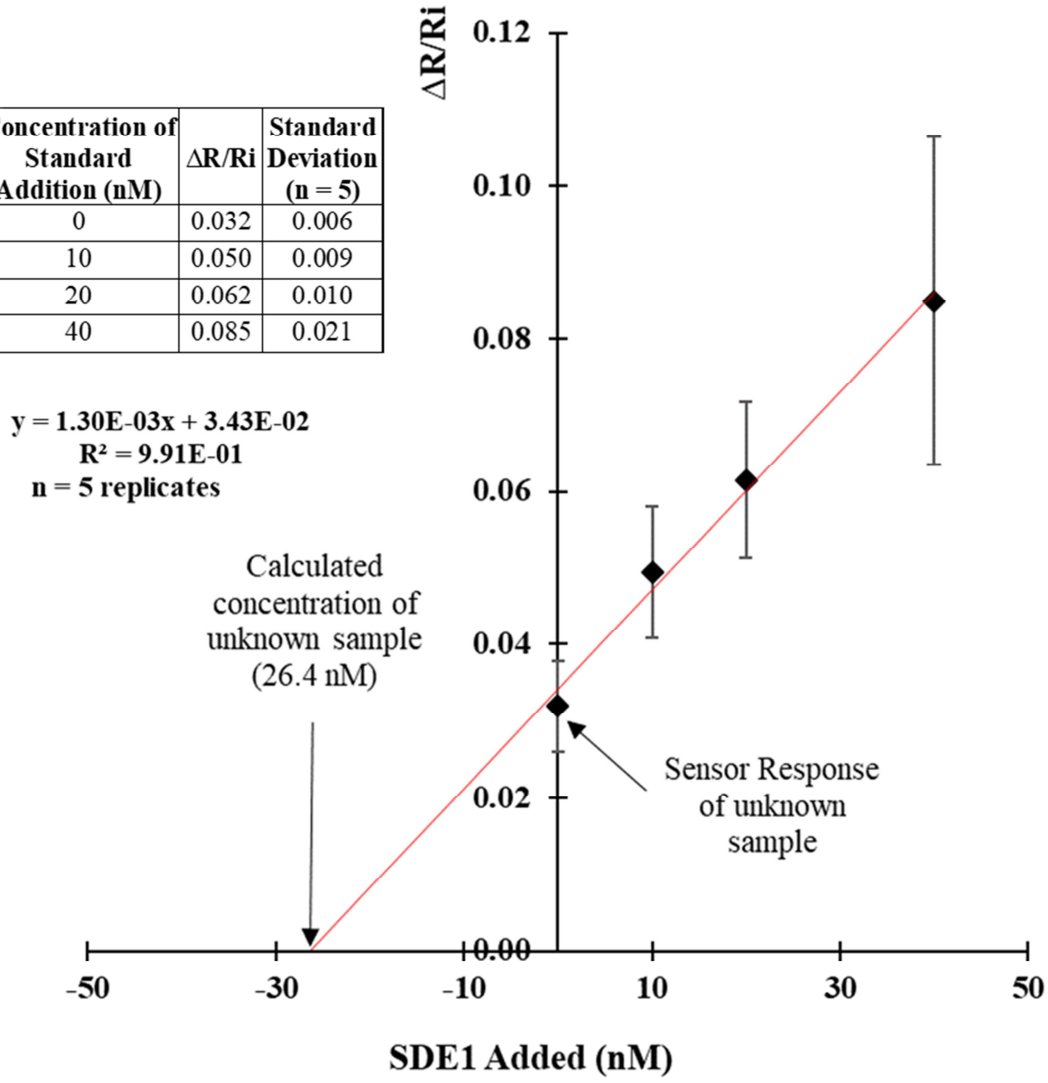

***Figure 6**: Determination of SDE1 concentration in simulated "unknown" plant extract sample, with actual concentration of 29.4 nM. Measured/determined SDE1 concentration of 26.4 nM is the absolute value of x-intercept of the fitted regression line in nanomolar. Error bars represent one standard deviation. Inset table shows standard SDE1 concentrations added to simulated unknown sample for analysis by the standard-addition method. $\Delta R/R_i$ and error bars (±1 standard deviations) were obtained from 5 individual sensors at each concentration.*

5 Conclusion

With the looming crisis caused by HLB disease, it is imperative that disease management strategies address the challenges associated with accurate, timely, and robust detection and

diagnosis of infected trees in order to curb the disease epidemic (Gottwald, 2010; Pagliaccia et al., 2017; Teixeira et al., 2008). This work presents a novel monitoring strategy based on the detection of secreted protein biomarker, SDE1, providing an additional tool to overcome challenges faced by other detection methods, such as nucleic acid-based assays and symptom-based detection which have been found prone to false negatives and mis-diagnoses (Pagliaccia et al., 2017). This research is the first of its kind to demonstrate label-free detection and quantification of SDE1 biomarkers for citrus greening using an SWNT-based chemiresistive biosensor. In our previous publication, we have demonstrated detection of SDE1 using an indirect enzyme-linked immunosorbent assay (ELISA) in the nanomolar range from 1.4 nM to 140 nM (Pagliaccia et al., 2017). The biosensor in the current research demonstrated a dynamic range in the nanomolar range from 3 nM to at least 2.6 µM. Furthermore, by adopting the standard additions assay method, we have demonstrated the feasibility of the biosensor to be used without requiring an external calibration curve.

While this work demonstrates the detection and quantification of the HLB biomarker, SDE1, in plant tissue using a chemiresistive biosensor, additional optimization for the sensor and sample preparation methods is required to meet the more rigorous demands for field application. Future work will address the engineering challenges to make the biosensors with lower inter-device variability, which can be achieved through optimization of scaled-up sensor fabrication processes (Gao et al., 2016; Ping et al., 2016). Additionally, to improve overall sensor limits of detection and stability, higher-affinity and more stable monoclonal anti-SDE1 antibodies can be developed and screened for use as the biorecognition element in the biosensor. In addition to small device footprint, another advantage of chemiresistive sensors is the simplicity of the accompanying measurement electronics, which can be a simple ohmmeter circuit. Combining

simple measurement circuits with low cost, off-the-shelf microcontrollers such as the Arduino open-source electronics platform, a portable biosensor system is achievable for field use (Hwang et al., 2019; Mathupala et al., 2016). Thus, a portable, facile, and label-free chemiresistive biosensor platform for detection of HLB biomarkers for field application will be an impactful addition to the current technology toolshed to curb the spread of citrus greening.

Acknowledgement

This work was supported by grants from U.S. Department of Agriculture (2014-67021-21589) to AM and WM and National Science Foundation (1606181 and 1842718) to AM. AM acknowledges the W. Ruel Johnson Chair in Environmental Engineering.

6 References

Andersen, J.E.T., 2017. TrAC Trends in Analytical Chemistry 89, 21–33.

Arredondo Valdés, R., Delgado Ortiz, J.C., Beltrán Beache, M., Anguiano Cabello, J., Cerna Chávez, E., Rodríguez Pagaza, Y., Ochoa Fuentes, Y.M., 2016. Can. J. Microbiol. 62, 803–811.

Balasubramanian, K., Burghard, M., 2006. Analytical and Bioanalytical Chemistry 385, 452–468.

Banerjee, S., Hemraj-Benny, T., Wong, S.S., 2005. Advanced Materials 17, 17–29.

Basu, J., Datta, S., RoyChaudhuri, C., 2015. Biosensors and Bioelectronics 68, 544–549.

Bové, J.M., 2006. Journal of plant pathology 7–37.

Byon, H.R., Choi, H.C., 2006. Journal of the American Chemical Society 128, 2188–2189.

Chen, R.J., Choi, H.C., Bangsaruntip, S., Yenilmez, E., Tang, X., Wang, Q., Chang, Y.-L., Dai, H., 2004. Journal of the American Chemical Society 126, 1563–1568.

Chen, X., Liu, Y., Fang, X., Li, Z., Pu, H., Chang, J., Chen, J., Mao, S., 2019. Biosensors and Bioelectronics 126, 664–671.

Chen, Y., Ren, R., Pu, H., Guo, X., Chang, J., Zhou, G., Mao, S., Kron, M., Chen, J., 2017. Sci Rep 7.

Chen, Z., Appenzeller, J., Knoch, J., Lin, Y., Avouris, P., 2005. Nano Letters 5, 1497–1502.

Choi, K.H., Bourgoin, J.P., Auvray, S., Esteve, D., Duesberg, G.S., Roth, S., Burghard, M., 2000. Surface Science 462, 195–202.

Conroy, P.J., Hearty, S., Leonard, P., O'Kennedy, R.J., 2009. Seminars in Cell & Developmental Biology, A Special Edition on Biosensors and Development of Pigment Cells and Pigment Patterns 20, 10–26.

Das, R., Dhiman, A., Kapil, A., Bansal, V., Sharma, T.K., 2019. Anal Bioanal Chem 411, 1229–1238.
Ding, F., Duan, Y., Paul, C., Brlansky, R.H., Hartung, J.S., 2015. PLoS One 10.
Ellison, S.L.R., Thompson, M., 2008. Analyst 133, 992.
Fakanya, W., Tothill, I., Fakanya, W.M., Tothill, I.E., 2014. Biosensors 4, 340–357.
Findlay, J.W.A., Dillard, R.F., 2007. AAPS J 9, E260–E267.
Gao, Z., Kang, H., Naylor, C.H., Streller, F., Ducos, P., Serrano, M.D., Ping, J., Zauberman, J., Rajesh, Carpick, R.W., Wang, Y.-J., Park, Y.W., Luo, Z., Ren, L., Johnson, A.T.C., 2016. ACS Applied Materials & Interfaces 8, 27546–27552.
García-Aljaro, C., Cella, L.N., Shirale, D.J., Park, M., Muñoz, F.J., Yates, M.V., Mulchandani, A., 2010. Biosensors and Bioelectronics 26, 1437–1441.
Georgakilas, V., Otyepka, M., Bourlinos, A.B., Chandra, V., Kim, N., Kemp, K.C., Hobza, P., Zboril, R., Kim, K.S., 2012. Chemical Reviews 112, 6156–6214.
Gottwald, T.R., 2010. Annual Review of Phytopathology 48, 119–139.
Graça, J.V. da, Douhan, G.W., Halbert, S.E., Keremane, M.L., Lee, R.F., Vidalakis, G., Zhao, H., 2016. Journal of Integrative Plant Biology 58, 373–387.
Hao, Z., Pan, Y., Shao, W., Lin, Q., Zhao, X., 2019. Biosensors and Bioelectronics 134, 16–23.
He, Q., Wu, S., Yin, Z., Zhang, H., 2012. Chemical Science 3, 1764.
Heller, I., Janssens, A.M., Männik, J., Minot, E.D., Lemay, S.G., Dekker, C., 2008. Nano Letters 8, 591–595.
Hu, P., Zhang, J., Li, L., Wang, Z., O'Neill, W., Estrela, P., 2010. Sensors 10, 5133–5159.
Hwang, S.I., Franconi, N.G., Rothfuss, M.A., Bocan, K., Bian, L., White, D.L., Burkert, S.C., Euler, R., Sopher, B.J., Vinay, M.L., Sejdic, E., Star, A., 2019. ACS Sens.
Iijima, S., 1991. Nature 354, 56–58.
Irey, M.S., Gast, T., Gottwald, T.R., 2006. Comparison of visual assessment and polymerase chain reaction assay testing to estimate the incidence of the Huanglongbing pathogen in commercial Florida citrus, in: Proc. Fla. State Hortic. Soc. pp. 89–93.
Jain, R., Miri, S., Pachapur, V.L., Brar, S.K., 2019. Chapter 14 - Advances in antibody-based biosensors in environmental monitoring, in: Kaur Brar, S., Hegde, K., Pachapur, V.L. (Eds.), Tools, Techniques and Protocols for Monitoring Environmental Contaminants. Elsevier, pp. 285–305.
Kaisti, M., 2017. Biosensors and Bioelectronics 98, 437–448.
Katz, H., 2004. Electroanalysis 16, 1837–1842.
Lee, C.-S., Kim, S.K., Kim, M., 2009. Sensors 9, 7111–7131.
Liu, J., Casavant, M.J., Cox, M., Walters, D.A., Boul, P., Lu, W., Rimberg, A.J., Smith, K.A., Colbert, D.T., Smalley, R.E., 1999. Chemical Physics Letters 303, 125–129.
Liu, S., Guo, X., 2012. NPG Asia Materials 4, e23.
Mathupala, S.P., Kiousis, S., Szerlip, N.J., 2016. PLoS One 11.
O'Connell, M.A., Belanger, B.A., Haaland, P.D., 1993. Chemometrics and Intelligent Laboratory Systems 20, 97–114.
Odom, T.W., Huang, J.-L., Kim, P., Lieber, C.M., 1998. Nature 391, 62–64.
Ohno, Y., Maehashi, K., Matsumoto, K., 2010. Biosensors and Bioelectronics 26, 1727–1730.
Ohno, Y., Maehashi, K., Matsumoto, K., 2015. Graphene Biosensor, in: Matsumoto, K. (Ed.), Frontiers of Graphene and Carbon Nanotubes. Springer Japan, Tokyo, pp. 91–103.
Okon, S.L., Ronkainen, N.J., 2017. Electrochemical Sensors Technology.

Pagliaccia, D., Shi, J., Pang, Z., Hawara, E., Clark, K., Thapa, S.P., Francesco, A.D., Liu, J., Tran, T.-T., Bodaghi, S., Folimonova, S.Y., Ancona, V., Mulchandani, A., Coaker, G., Wang, N., Vidalakis, G., Ma, W., 2017. Frontiers in Microbiology 8.
Ping, J., Vishnubhotla, R., Vrudhula, A., Johnson, A.T.C., 2016. ACS Nano 10, 8700–8704.
Ramnani, P., Gao, Y., Ozsoz, M., Mulchandani, A., 2013. Analytical Chemistry 85, 8061–8064.
Sankaran, S., Mishra, A., Ehsani, R., Davis, C., 2010. Computers and Electronics in Agriculture 72, 1–13.
Sarkar, A., Daniels-Race, T., 2013. Nanomaterials (Basel) 3, 272–288.
Saylan, Y., Yilmaz, F., Özgür, E., Derazshamshir, A., Yavuz, H., Denizli, A., 2017. Sensors 17, 898.
Sharma, S., Byrne, H., O'Kennedy, R.J., 2016. Essays Biochem 60, 9–18.
Sun, Y.-P., Fu, K., Lin, Y., Huang, W., 2002. Accounts of Chemical Research 35, 1096–1104.
Teixeira, D.C., Saillard, C., Couture, C., Martins, E.C., Wulff, N.A., Eveillard-Jagoueix, S., Yamamoto, P.T., Ayres, A.J., Bové, J.M., 2008. Molecular and Cellular Probes 22, 139–150.
Terse-Thakoor, T., Ramnani, P., Villarreal, C., Yan, D., Tran, T.-T., Pham, T., Mulchandani, A., 2019. Biosensors and Bioelectronics 126, 838–844.
Thévenot, D.R., Toth, K., Durst, R.A., Wilson, G.S., 2001. Biosensors and Bioelectronics 16, 121–131.
Tlili, C., Myung, N.V., Shetty, V., Mulchandani, A., 2011. Biosensors and Bioelectronics 26, 4382–4386.
Tran, T.-T., Mulchandani, A., 2016. TrAC Trends in Analytical Chemistry 79, 222–232.
Tyler, H.L., Roesch, L.F.W., Gowda, S., Dawson, W.O., Triplett, E.W., 2009. MPMI 22, 1624–1634.
Wasik, D., Mulchandani, A., Yates, M.V., 2018. Anal. Chem. 90, 679–684.
Watson, T.J., 2007. Nature Nanotechnology 2.

Highlights:

- Label-free biosensor for secretory biomarker of citrus greening was developed.
- Single-walled carbon nanotubes (SWNTs) were used as chemiresistive transducer.
- Polyclonal antibodies were used as the biorecognition element.
- The sensor was sensitive and specific, with 5-nM detection limit in plant extract.
- Quantitative detection in plant extract was attained with standard addition method.

CRediT Author Statement:

Ms. Ref. No.: BIOS-D-19-02377

Thien-Toan Tran: Conceptualization, Methodology, Software, Formal Analysis, Investigation, Writing – Original Draft, Writing – Review & Editing, Visualization. **Kelley Clark**: Investigation, Resources, Writing – Review & Editing. **Wenbo Ma**: Conceptualization, Methodology, Resources, Supervision, Project Administration, Funding Acquisition. **Ashok Mulchandani**: Conceptualization, Methodology, Resources, Writing – Review & Editing, Supervision, Project Administration, Funding Acquisition.

Declaration of interests

☒ The authors declare that they have no known competing financial interests or personal relationships that could have appeared to influence the work reported in this paper.

☐The authors declare the following financial interests/personal relationships which may be considered as potential competing interests: